Computers and Chemical Engineering 34 (2010) 643–655

Contents lists available at ScienceDirect

Computers and Chemical Engineering

journal homepage: www.elsevier.com/locate/compchemeng

Advanced control for fuel cells connected to a DC/DC converter and an electric motor

D. Zumoffen [1], M. Basualdo [*,1]

Group of Applied Informatics to Process Engineering (GIAIP), Centro Franco-Argentino de Ciencias de la Información y de Sistemas (CIFASIS-CONICET-UNR-UPCAM III), 27 de Febrero 210 bis, S2000EZP Rosario, Argentina

ARTICLE INFO

Article history:
Received 30 July 2009
Received in revised form 30 October 2009
Accepted 2 November 2009
Available online 13 November 2009

Keywords:
Fuel cell
Predictive adaptive robust control
DC/DC converter
Electric motor

ABSTRACT

The transient behavior of a polymer electrolyte membrane fuel cells (PEMFC) system under an improved adaptive predictive control with robust filter (APCWRF) is analyzed using a nonlinear dynamic, control-oriented model. Sudden changes in the stack current are associated with the abrupt changes in the power demanded by the electric motor of a vehicle, powered by the PEMFC. The APCWRF is designed for controlling the compressor motor voltage. Because of the wide working range the control algorithm is improved accounting three different zones supported by three nominal models. It is specially thought to achieve a better efficiency and to maintain the necessary level of the oxygen in the cathode to prevent short circuit and membrane damage. A DC/DC converter is connected to the electric motor. It is used as an actuator in a cascade control loop to regulate the torque output of a DC electric motor with a PI controller in the external loop. Several results are presented considering the PEMFC with the APCWRF showing its potentiality for a wide working range imposed by two types of DC motors.

1. Introduction

Fuel cells are devices that convert chemical energy (often in the form of hydrogen) into electricity, without passing through a combustion stage. Whereas few fuel cell-based devices are currently available to the consumers, they have the potential to be used, in different layouts and types, to provide electric power to diverse utilities.

Research in dynamics and control of fuel cells is practically incipient and claims to receive more and more attention. Among some interesting contributions can be mentioned the work of Pukrushpan, Stefanopoulou, and Peng (2004) which presented a complete dynamic model of the PEMFC and their auxiliary systems. In addition, a complete set of nonlinear static relationships are given to an optimal FC operation according to the load demands. In Benziger, Chia, Moxley, and Kevrekidis (2005) and Woo and Benziger (2007) the complex dynamics of PEM operation and a feedback control strategy are discussed respectively. The first work analyzed the PEM behavior associated with the membrane water uptake, and the second one presented an approach to control the power output using limitations in the hydrogen feed to the fuel cell. This type of regulation could be beneficial for small fuel cell systems where recycling unreacted hydrogen may be impractical. On the other hand, Jayasankar, Ben-Zvi, and Huang (2009) presented an identifiability and estimation analysis for a dynamic model of a solid oxide fuel cell. The identifiability was tested by partitioning the main model into four sub-models and the estimability of the model was studied using sensitivity analysis under different external load profiles. In Zenith and Skogestad (2007) a simplified dynamic model for fuel cells was developed. They derived a theorem that indicates the conditions under which the power output of fuel cells can be, in theory, perfectly controlled. A fuel cell connected to a DC/DC converter is numerically simulated , with a control system based on switching rules in order to control the converter's output voltage. Caux, Lachaize, Fadel, Shott, and Nicod (2005) considered a system comprising a fuel cell, a compressor, valves and two DC/DC converters. The analysis of the complete system is a step forward from the studies where the fuel cell had been seen as a separate entity from the rest of the process. Recently, in the works of Biset, Nieto Deglioumini, Basualdo, Garcia, and Serra (2009) and Nieto Deglioumini, Biset, Domínguez, and Basualdo (2009) have been analyzed the control problem of the PEMFC in the context of a plant-wide control structure for the process of Hydrogen production from bio-ethanol accounting steady-state information only.

Some approaches proposed advanced control strategies on the PEMFC. Wua, Xu, and Hwang (2009) proposed a multi-loop nonlinear predictive control with constraints to guarantee a safe operation as well as long lifetime of the fuel cell in a hybrid system. Basically, the authors suggested the stack temperature and oxygen excess

* Corresponding author. Tel.: +54 0341 4237248x304.
E-mail addresses: zumoffen@cifasis-conicet.gov.ar (D. Zumoffen), basualdo@cifasis-conicet.gov.ar (M. Basualdo).
[1] Also with Universidad Tecnológica Nacional (UTN) Fac. Reg. Rosario (FRRo), Zeballos 1341, S2000BQA Rosario, Argentina.

0098-1354/$ – see front matter © 2009 Elsevier Ltd. All rights reserved.
doi:10.1016/j.compchemeng.2009.11.001

Nomenclature

Acronyms

APC	adaptive predictive control
APRF	adaptive predictive robust filter
APCWRF	adaptive predictive control with robust filter
CV	controlled variables
D	disturbances
DC	direct current
FB	feedback
FC	fuel cell
FF	feedforward
FIR	finite impulse response
ICV	indirect controlled variable
LS	least square
MV	manipulated variable
OD	oxygen demand
PEMFC	polymer electrolyte membrane FC
PMDC	permanent magnet DC
PVs	performance variables
SEDC	separate excited DC
TCS	traction control system

Variables

$\mathbf{A}$	penalty matrix
$\mathbf{B}$	penalty matrix
$\widehat{cgl}$	plant parameter
d	process delay
D_0	nominal controller denominator
D^*	controller denominator
$\mathbf{D}_*$	UD-factorization
e	tracking error
emf	electromotive force
emf_{ref}	electromotive force reference
$\tilde{e}$	a priori prediction error
$\hat{g}(i)$	estimated FIR component
G	plant FIR model
$\hat{G}$	estimated FIR model
G_0	nominal FIR model
$\mathbf{G}$	dynamic matrix
H_p	prediction horizon, end
H_u	control horizon
H_w	prediction horizon, begining
I_a	armature current
$I_{a,ref}$	armature current reference
I_e	excitation circuit current
$I_{e,ref}$	excitation current reference
I_{st}	stack current
J	functional cost
J_{cp}	compressor inertia
K_g	static compensation
m_{H_2}	hydrogen mass (anode)
m_{N_2}	nitrogen mass (cathode)
m_{O_2}	oxygen mass (cathode)
m_{sm}	air mass (supply manifold)
$m_{w,an}$	water mass (anode)
$m_{w,ca}$	water mass (cathode)
N	FIR order
p_{rm}	return manifold pressure
p_{sm}	supply manifold pressure
P_{cm}	power compressor motor
P_{cp}	compressor power load
P_{net}	net power
P_{net}^{max}	maximum net power
R	noncausal polinomial
R_a	air gas constant
R_0	nominal noncausal polinomial
s_1	supervision indicator
$\mathbf{S}$	dynamic matrix
t	time
$T_{cp,out}$	compressor exit air temperature
T_l	load torque
T_{rm}	return manifold gas temperature
T_{sm}	supply manifold gas temperature
$\mathbf{T}_i$	transformation matrix
u	manipulated variable
$\hat{u}$	estimated manipulated variable
u_{00}	operation point
U_a	armature voltage
U_e	excitation circuit voltage
$\mathbf{U}_*$	UD-factorization
v_{cm}	compressor voltage
v_{cm}^{opt}	optimal compressor voltage
v_{ref}	voltage reference for DC converter
V_{rm}	return manifold volume
V_{sm}	manifold volume
w	original set point
W_i	mass flow
W_{cp}^{opt}	optimal compressor air flow
y	plant output
y_{00}	operation point
$\hat{y}$	estimated plant output
y_r	reference signal
z_N	supervision indicator

Greek symbols

$\widehat{\Delta G}$	process-model mismatch estimation
α_i	penalty coefficients
α_r	filter smoothing coefficient
β_i	penalty coefficients
ε	prediction error
$\hat{\eta}$	disturbance estimation
$\hat{\theta}$	estimation parameters
$\hat{\theta}_N^{LS}$	LS estimation parameters
λ	forgetting factor
λ_{O_2}	oxygen excess ratio
$\lambda_{O_2}^{opt}$	optimal oxygen excess ratio
ψ	regressor vector
ω_{cp}	compressor speed
ω_{ref}	shaft speed reference
ω_s	shaft DC motor speed

ratio in the cathode as controlled variables and the compressor air flow and water flow rate as manipulated variables. On the other hand, a SISO model-based predictive control is presented by Gruber, Doll, and Bordons (2009) to regulate the oxygen excess ratio. The methodology was tested by experimental results. A few adaptive control strategies have been proposed too. In Zhang, Liu, Yu, and Ouyanga (2008) an adaptive control algorithm (ARMAX model-based) was presented to dynamically stabilize the oxygen excess ratio around an optimal level. This adaptive control was evaluated on a test bench. In this case it was not shown a wide range of operation for the FC. Yang, Liu, and Wang (2008) presented an application of a model reference adaptive control to a low-power PEM fuel cell system. It provided a strategy for regulating the voltage and current of the fuel cell by adaptively adjusting the flow rates

of air and hydrogen. The control approach used adaptive ARMA models.

In this work the feedforward actions are improved by an adaptive feedback structure. The operational conditions for the PEMFC were adopted from the recommendations given by Pukrushpan et al. (2004), Grujicic, Chittajallu, Law, and Pukrushpan (2004) and Grujicic, Chittajallu, and Pukrushpan (2004). The focus of this paper consists on the regulation of the air supply to the cathode, which is the controlled variable, even though a wide range of disturbances in current demands, from different kind of the electric motors, are performed. The optimal value of the compressor motor voltage (manipulated variable) which maximizes the stack net power and an optimal value of oxygen demand (OD) at each level of stack current are taken from Pukrushpan et al. (2004). In this context, it is designed an adaptive predictive control with robust filter (APCWRF) by zones combined with a feedforward action for improving the regulation behavior when the disturbances are produced by the DC/DC converter connected to the electric motor. Initially, the APCWRF approach was proposed by Jordán (1991) and Jordán, Basualdo, and Zumoffen (2006), lately, some modifications were performed by Zumoffen, Basualdo, Jordán, and Ceccatto (2007) to turn it as a fault-tolerant control. This strategy guarantees a suitable FC operation in a wide range and solves the nonlinear behavior problems by means of an adaptive control approach. In addition, indirectly the net power output (performance variable) delivered to a DC motor from a FC through a DC/DC converter can be controlled too. The APCWRF by zones is based on three FIR nominal models that represent the operating zones available for the FC current stack (100–280 A). Thus, the zone that is set by the corresponding current demand, a suitable nominal FIR model is selected according to it and the APCWRF algorithm updates both the controller and the model properly. The overall controller design and the corresponding synchronization indicators (model or controller update) are detailed here. Several simulated results are presented for both permanent magnet DC (PMDC) motor and separately excited DC (SEDC) motor under arbitrary load profiles in the traction control system (TCS).

2. The PEMFC model

The nonlinear dynamic model developed by Pukrushpan et al. (2004) is based on electrochemical, thermodynamic and zero-dimensional fluid mechanics principles. Basically, the slower dynamics associated with temperature regulation and heat dissipation are avoided and is focussed in the reactant pressure and flow behavior. Here, it is also assumed as well regulated the stack average temperature and the inlet reactant flows in the cathode and anode. In addition, it is considered that they are humidified, heated and cooled in a consistent and rapid way. Thus, the dynamic model has a state-space representation with nine sates as can be observed through Eqs. (1)–(9). The principle of the mass conservation applied in the cathode is given by Eqs. (1)–(3) for the oxygen, nitrogen and water respectively. Similarly, the governing equations for hydrogen and water in the anode are given by Eqs. (4) and (5). The dynamic of air supercharging device is governed by the compressor inertia in Eq. (6) with $J_{cp} = 5 \times 10^{-5}$ kg/m^2. The rate of change of mass inside the manifold and the rate of change of supply manifold pressure are given by Eqs. (7) and (8) using the principle of mass and energy conservation respectively, where R_a represents the air gas constant. Finally, the return manifold pressure is governed by the mass conservation and the ideal gas law through isothermic assumptions given by Eq. (9).

$$\dot{m}_{O_2} = W_{O_2,in} - W_{O_2,out} - W_{O_2,react} \quad (1)$$

$$\dot{m}_{N_2} = W_{N_2,in} - W_{N_2,out} \quad (2)$$

$$\dot{m}_{w,ca} = W_{v,ca,in} - W_{v,ca,out} + W_{v,gen} + W_{v,mbr} \quad (3)$$

$$\dot{m}_{H_2} = W_{H_2,in} - W_{H_2,purge} - W_{H_2,react} \quad (4)$$

$$\dot{m}_{w,an} = W_{v,an,in} - W_{v,an,out} + W_{v,mbr} \quad (5)$$

$$J_{cp}\dot{\omega}_{cp} = \frac{P_{cm} - P_{cp}}{\omega_{cp}} \quad (6)$$

$$\dot{m}_{sm} = W_{cp} - W_{ca,in} \quad (7)$$

$$\dot{p}_{sm} = \frac{\gamma R_a (W_{cp} T_{cp,out} - W_{ca,in} T_{sm})}{V_{sm}} \quad (8)$$

$$\dot{p}_{rm} = \frac{R_a T_{rm} (W_{ca,out} - W_{rm,out})}{V_{rm}} \quad (9)$$

The compressor air mass flow rate is modelled by the nonlinear curve fitting method and the compressor motor dynamic, resulting a function of the compressor motor input voltage and the supply manifold pressure, $W_{cp} = f(v_{cm}, p_{sm})$. The thermodynamic equations are used to calculate the exit air temperature, $T_{cp,out}$ and the required compressor power, P_{cp}. The air flow rate in and out of the cathode ($W_{ca,in}$, $W_{ca,out}$) are functions of the difference between the pressure of the gas upstream and downstream, and are approximated by a linear nozzle equation $W = k(p_1 - p_2)$. The flow rates of each element (O_2, N_2, vapor) are determined using thermodynamic and psychrometric properties of the gas upstream. The return manifold exit flow rate, $W_{rm,out}$, is calculated using nonlinear nozzle equation for accounting possible large pressure drops. The rates of oxygen and hydrogen reacted and the water generated are function of the stack current (using electrochemical relationships), $W_{O_2,react} = k_o I_{st}$, $W_{H_2,react} = k_h I_{st}$ and $W_{v,gen} = k_w I_{st}$ respectively. Where, k_o, k_h and k_w take into account the number of cells, the Faraday number and the molar mass for each component. The mass flow of vapor across the membrane, $W_{v,mbr}$, is calculated using mass transport principles and the membrane properties. The main variables are summarized in the nomenclature section.

2.1. Fuel cell net power

The net power of a fuel cell system, P_{net}, can be approximately defined as the difference between the power produced by the stack, P_{st}, and the required power to run the air compressor motor, P_{cm}. At a given stack current I_{st}, corresponds a determined compressor input voltage v_{cm} related to both the compressor air mass flow rate and the excess amount of oxygen $\lambda_{O_2} = W_{O_2,in}/W_{O_2,react}$ in the cathode. However, it must be noted that an increment in λ_{O_2} generally requires an excessive increment in v_{cm} which causes a P_{net} diminution. Thus, at each level of I_{st} there is an optimal value of $\lambda_{O_2}^{opt}$ at which the net power takes the maximum value P_{net}^{max}. Solving Eqs. (1)–(9) under steady-state condition, the optimal relationships can be found according to the different stack current values. Eqs. (10)–(13) summarize the optimal nonlinear mapping of the most important variables when the fuel cell operates under standard conditions 100 A$\leq I_{st} \leq$ 280 A (Pukrushpan et al., 2004). The complete model parameters can be found in Pukrushpan et al. (2004), Grujicic, Chittajallu, Law, et al. (2004), and Grujicic, Chittajallu, and Pukrushpan (2004).

$$v_{cm}^{opt} = -1.36 \times 10^{-3} I_{st}^2 + 1.17 I_{st} + 14.3 \quad (10)$$

$$W_{cp}^{opt} = -4.01 \times 10^{-7} I_{st}^2 + 4.03 \times 10^{-4} I_{st} - 1.5 \times 10^{-3} \quad (11)$$

$$\lambda_{O_2}^{opt} = -2.76 \times 10^{-6} I_{st}^2 - 15.93 \times 10^{-4} I_{st} + 2.73 \quad (12)$$

$$P_{net}^{max} = -2.99 \times 10^{-4} I_{st}^2 + 0.27 I_{st} - 0.87 \quad (13)$$

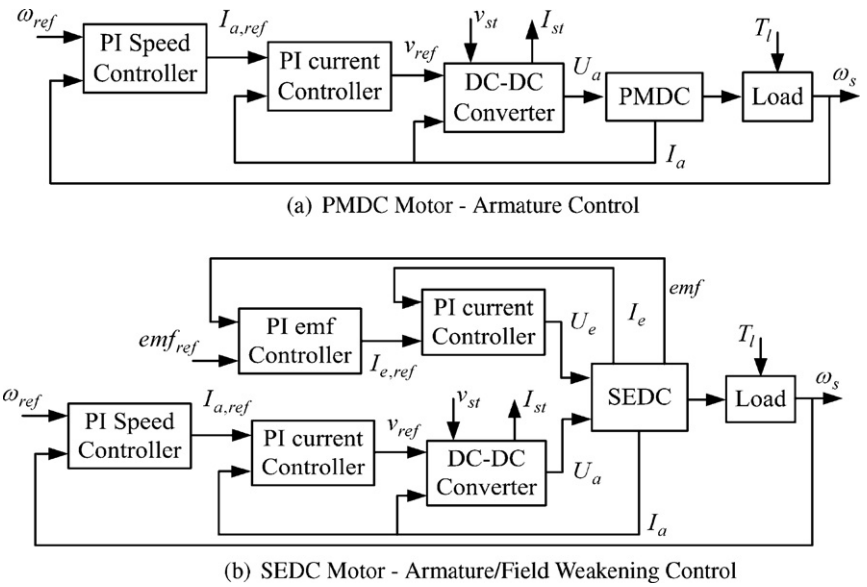

Fig. 1. Speed control strategies for DC motors. (a) PMDC motor: armature control and (b) SEDC motor: armature/field weakening control.

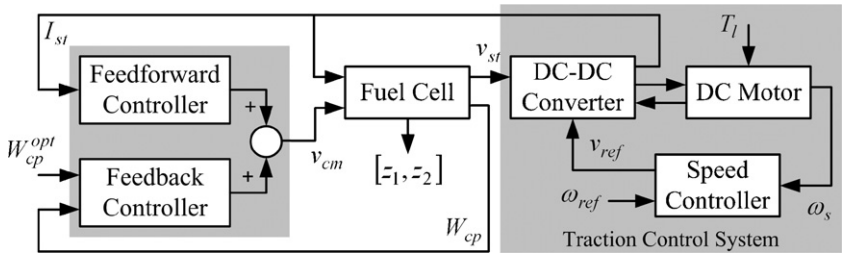

Fig. 2. Overall control structure of PEMFC and traction system.

3. Control problem formulation

In a FC system, there are three main control systems that regulate: (a) the air/fuel supply; (b) the water supply; and (c) the heat management. The main assumptions are: a perfect air/fuel humidifier and perfect air and stack cooler. In addition, a fast proportional feedback fuel-flow controller, which ensures a zero pressure difference across the membrane, is assumed. Therefore, the control problem discussed in the present work focuses on the regulation of the air (i.e. oxygen) supply to the cathode. From Eq. (10) can be observed the optimal value of the compressor motor voltage v_{cm}^{opt} which maximizes the stack net power, P_{net}^{max}. It was found quite successfully to represent the variation of the optimal v_{cm}^{opt} with I_{st}. When the current demand from the vehicle suddenly increases, the oxygen consumption in the cathode increases too producing that the oxygen partial pressure drops. The accompanying drop in the FC voltage may lead to a short circuit and/or membrane damage, the phenomenon is known as oxygen starvation. To prevent this from happening, the air supply must be promptly increased to replenish the cathode with oxygen. Also, the fuel supplied to the anode must be quickly adjusted to ensure a minimal pressure difference across the FC membrane. A similar control of the FC system is required during a sudden drop in the stack current. Thus, the FC system control problem can be defined as:

- Manipulated variable (MV): compressor input voltage, v_{cm}.
- Controlled variable (CV): compressor air mass flow rate, W_{cp}.
- Disturbance (D): stack current, I_{st}.
- Performance variables (PVs): power net difference, $z_1 = P_{net} - P_{net}^{max}$ and excess ratio difference, $z_2 = \lambda_{O_2} - \lambda_{O_2}^{opt}$.

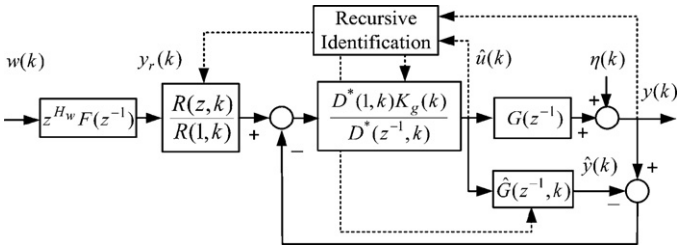

Fig. 3. Adaptive predictive control (APC) structure.

3.1. Disturbances to the PEMFC

The DC motors considered here present different excitation modes (field coil connections), and eventually different control structures as shown in Fig. 1.

Case 1: Permanent magnet DC (PMDC) motor. In this case the poles are formed by a permanent magnet with constant magnetic flux. A cascade control structure is used for the speed control (master loop) that gives the current reference signal, $I_{a,ref}$, for the induced current controller (slave). In addition, this current controller has to define the induced voltage feed, v_{ref}, for the DC/DC converter. The overall control structure can be observed in Fig. 1(a).

Case 2: Separately excited DC (SEDC) motor. In this case the field circuit (I_e, U_e) is excited independently of the armature circuit (I_a, U_a) and the speed control can manipulate both armature and excitation voltage. Basically, a combined strategy is proposed

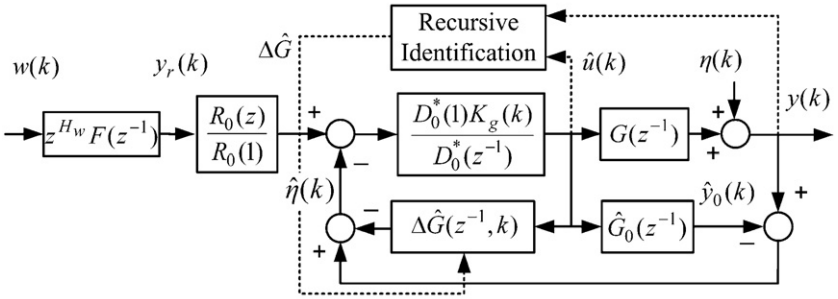

Fig. 4. Adaptive predictive robust filter (APRF) structure.

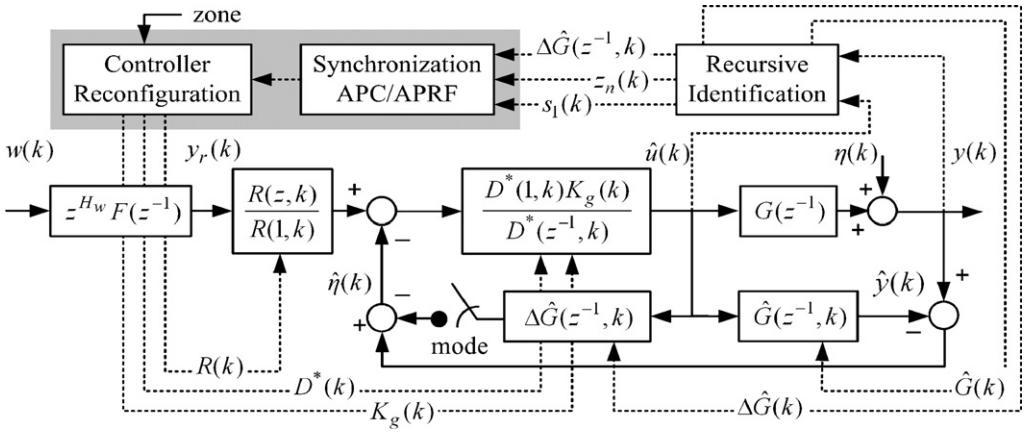

Fig. 5. Adaptive predictive control with robustness filter (APCWRF) structure.

here allowing to operate the DC machine in both nominal and over-speed (field weakening) zones. In this control structure can be observed two control loops. By one hand, the armature loop, containing a current control of the internal armature and an external speed controller connected in cascade. By other hand, the excitation loop, that also presents two hierarchical cascade controllers: the internal excitation current controller and the external electromotive force (emf) controller. This control structure can be observed in Fig. 1(b).

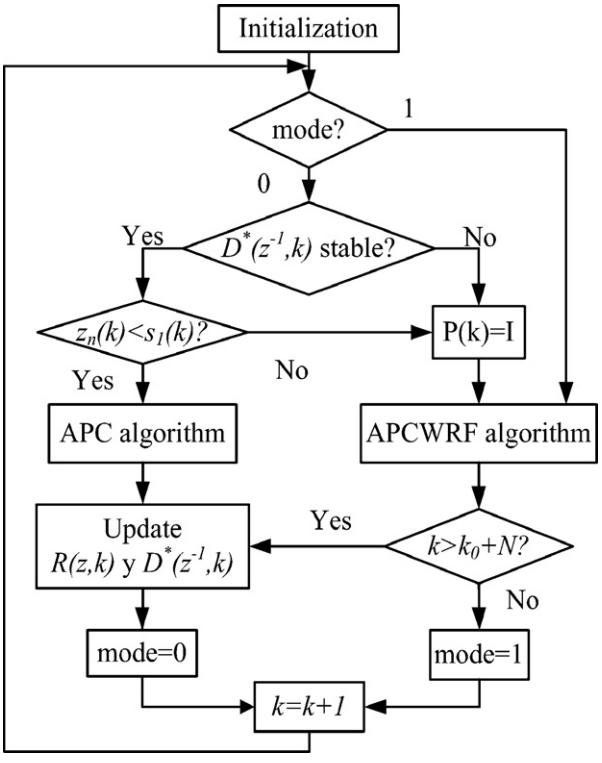

Fig. 6. APCWRF synchronization algorithm.

All the controllers used in these subsystems are PI type with anti-windup. The currents and voltages in the armature and excitation circuits are limited considering their maximum allowed time of currents overshoot and 1.2 times the nominal value for voltages.

The only way to control the speed in PMDC motors is by means of the armature circuit (the field excitation is fixed). The zone in which the excitation is constant and the armature voltage, U_a, can be modified is generally called the *constant torque region*. The maximum value for, U_a, is given by its nominal magnitude, U_{aN}, generates the nominal speed, ω_N, the maximum achievable speed in these conditions. On the other hand, the SEDC motors have an additional circuit with implications on the speed, the excitation circuit. It allows to achieve different degrees of the excitation in an independent way. Then, in SEDC motors the speed can achieve higher values than the nominal one by means of a suitable excitation field weakening procedure. This approach defines the so called *constant power region*, due to both the armature voltage and current at the nominal magnitudes. The above stated regions are common in DC machines analysis by using the capability curves. Based on this, the speed control structure with both armature and excitation circuit manipulations present flexibility in the operational range.

The control structures shown in Fig. 1 are the load effect connected to PEMFC. This load is represented by the stack voltage, v_{st}, and the current stack, I_{st}. Thus, different range of operation for the DC motors represent different load scenarios from the PEMFC point of view.

In Fig. 2 the overall system with its control structure is summarized. Basically, it consists of the fuel cell with its local controllers (feedforward and feedback) connected to the DC–DC converter, the

Table 1
APCWRF parameter adjustment.

	Variable								
	H_w (samp.)	H_p (samp.)	H_u (samp.)	N	α_r	**A**	**B**	λ	T_s (s)
Value	1	11	2	30	0.09	**I**	**0**	0.995	0.1

DC motor as load disturbance and the speed controller constituting the traction control system (TCS). The load disturbance T_l (Nm), that affects the TCS, presents an arbitrary temporal profile as can be observed in Eq. (14). The DC motor reaches the desired speed without load ($t < 30$ s), avoiding an excessive fuel cell current transient requirements in this period.

$$T_l = \begin{cases} 0, & t < 30\,\text{s} \\ 30, & 30\,\text{s} \le t < 60\,\text{s} \\ 75, & 60\,\text{s} \le t < 90\,\text{s} \\ 30, & 90\,\text{s} \le t < 120\,\text{s} \\ 60, & t \ge 120\,\text{s} \end{cases} \tag{14}$$

In this work the proposed control structure performs two different actions. One of them considers the feedforward contribution given by an optimal static nonlinear mapping according to Eq. (10), and the second one takes into account the feedback contribution given by an adaptive predictive control (APC) by zones strategy. This last approach provides the suitable servo behavior for the optimal compressor air flow reference (Eq. (11)) manipulating the compressor input voltage. Thus, the optimal excess ratio of oxygen and the maximum net power are guaranteed even though the disturbances and plant-model mismatch occur. In the following section the feedback APC approach is detailed.

4. Adaptive predictive control by zones with robust filter

The main control structure used here involves a commutation between a linear time-varying robustness filter (RF) in the feedback path of the control loop and an adaptive predictive controller (APC). The decision of which of both modes has to work is based on specific indicators deeply described in Jordán et al. (2006). They are closely related to the operation conditions, which are checked every sampling time. This strategy is developed in a modular way composed by two stages. On one side, the good asymptotic performance of the

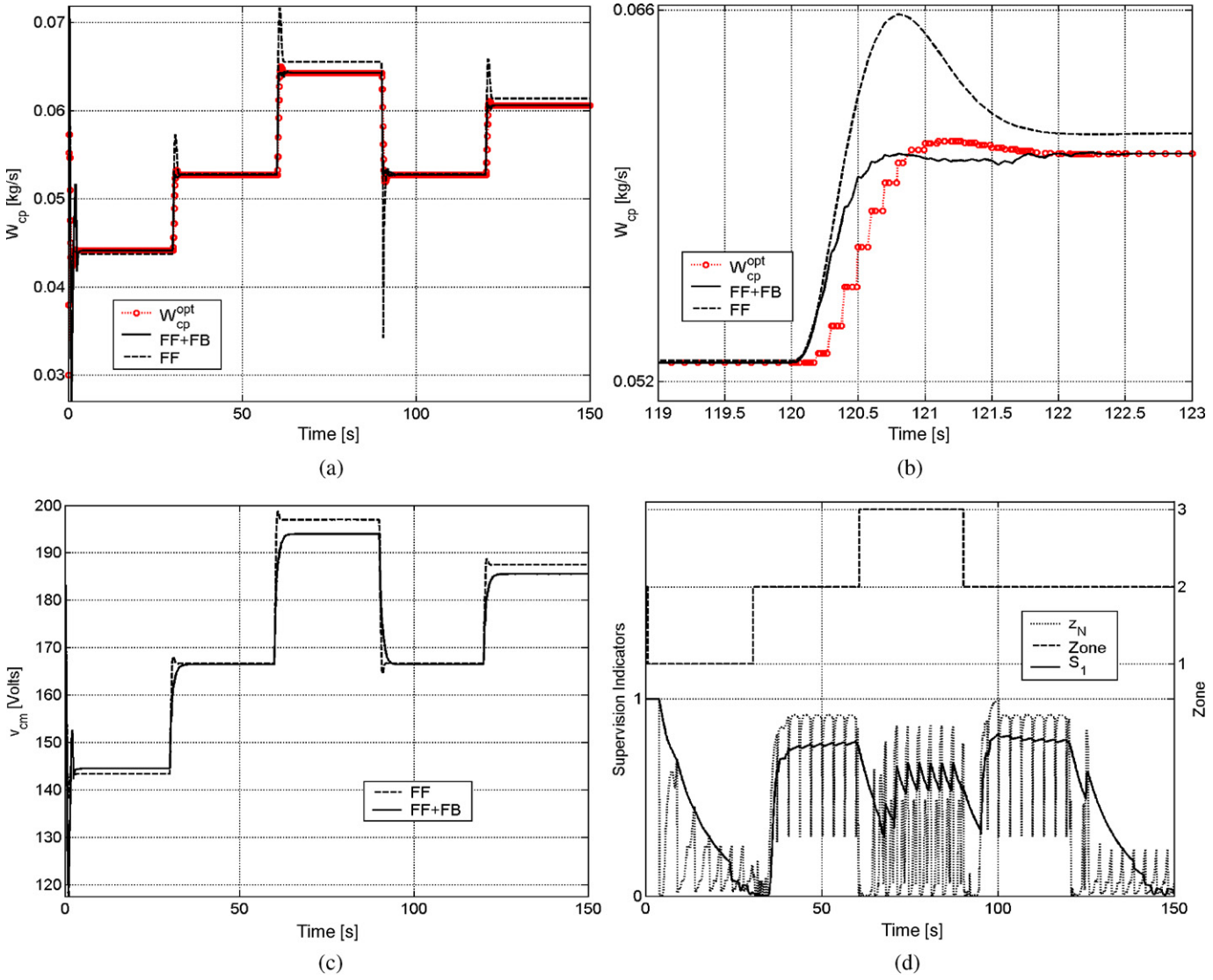

Fig. 7. Controller variables – PMDC motor. (a) Compressor air flow, (b) compressor air flow with zoom, (c) compressor motor voltage, and (d) indicators and zone.

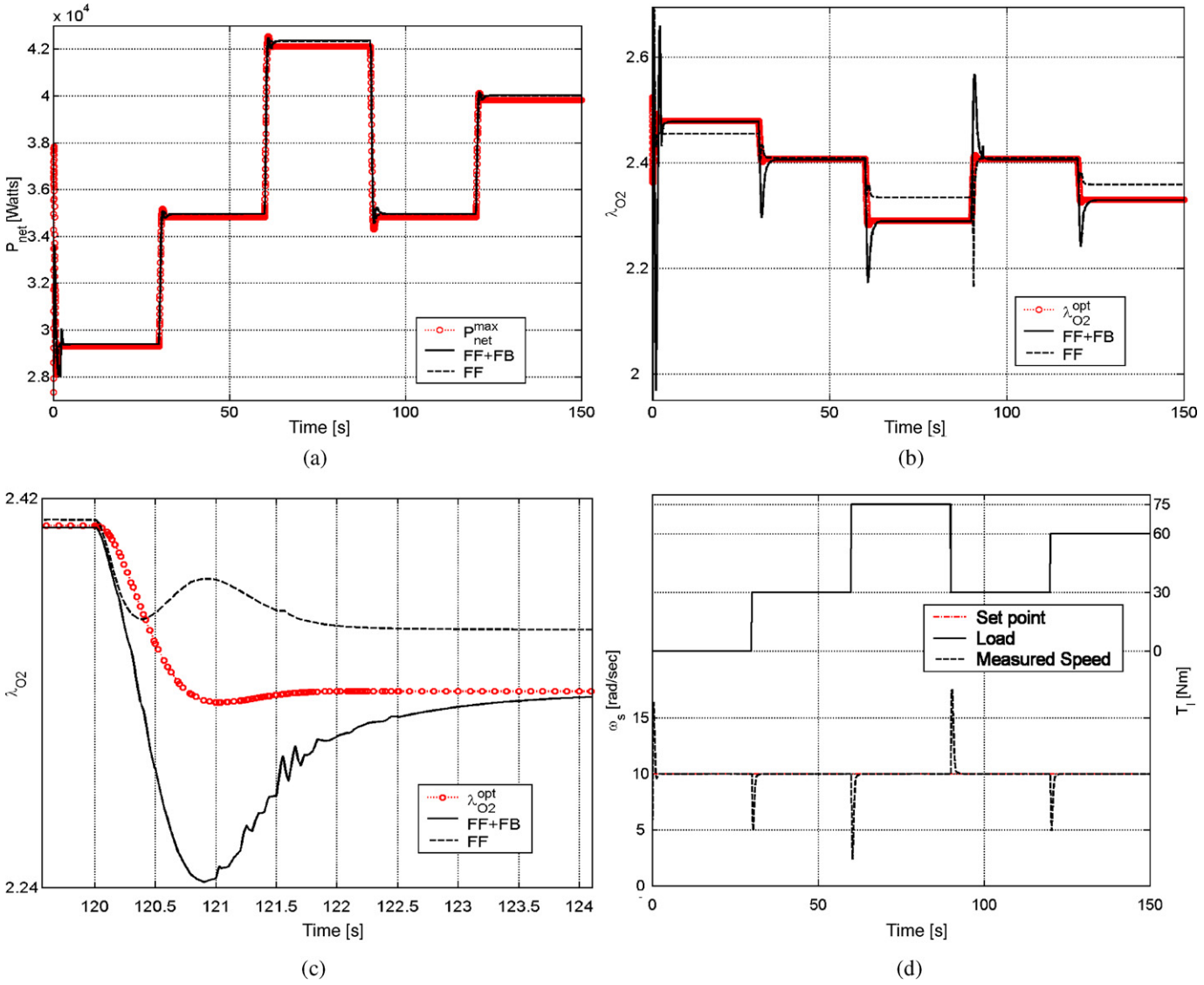

Fig. 8. Performance and load variables – PMDC motor. (a) Net power, (b) excess ratio, (c) excess ratio with zoom, and (d) shaft speed and torque.

APC system is reached. On the other side, the adaptive robustness filter (APRF) is accounted if sudden dynamic changes affect significantly the closed-loop behavior and APC cannot achieve good performance in these cases. The principal advantage of using this methodology is that a stable asymptotic behavior without extra tuning parameters is always achieved. The convergence and stability of the control system is analyzed in detail in Jordán (1991) and Jordán et al. (2006). According to the specific case study presented in this work, it was considered advantageous introducing some modifications to the original algorithm given the publications cited above. Hence, three FIR models, obtained around three strategic operating points inside the corresponding ranges: zone 1: 100–150 A, zone 2: 150–200 A, and zone3: 200–250 A. The initial conditions for each zone were taking into account in the control algorithm so as to be switched together in the transition stages. This modification gave an interesting improvement on the dynamic behavior for the wide working range imposed by the electric motors considered here respect to the older version of this control strategy given in Jordán et al. (2006). This issue justifies the name of the modified algorithm identified as *by zones* since each of the FIR model is enough representative for each corresponding working range.

4.1. Adaptive predictive approach

Consider a single input, single output system with linearizable dynamic for every operation point in the working region. Therefore the predictive controller structure can be obtained by minimizing the energy criterion in Eq. (15) applied at every step k.

$$J(k) = \sum_{i=H_w}^{H_p} \alpha_i^2 e^2(k+i) + \sum_{i=0}^{H_u-1} \beta_i^2 \hat{u}^2(k+i) \tag{15}$$

where $e(k)$ is a tracking error between a desired trajectory $y_r(k)$ and the predicted system output $\hat{y}(k)$ evaluated on the so-called prediction horizon $[H_w, H_p]$ via model, $y(k)$ corresponds to the past values of the system output and $\hat{u}(k)$ is the control action; been $\hat{u}(k)$ the calculated future control action over the so-called control horizon $[0, H_u - 1]$. Eq. (15) can consider the restrictions on $y(k)$ and $\hat{u}(k)$. The future output trajectory is originally calculated by means of a FIR model (finite impulse response: $\hat{g}(i), i = 1, \ldots, N$) of the system. The optimal control sequence $\hat{u}(k)$ can be easily deduced for the unconstrained case by searching for the global minimum of $J(k)$ with respect to $\hat{u}(k)$ over H_u. As the functional of Eq. (15) is quadratic, the minimum can be

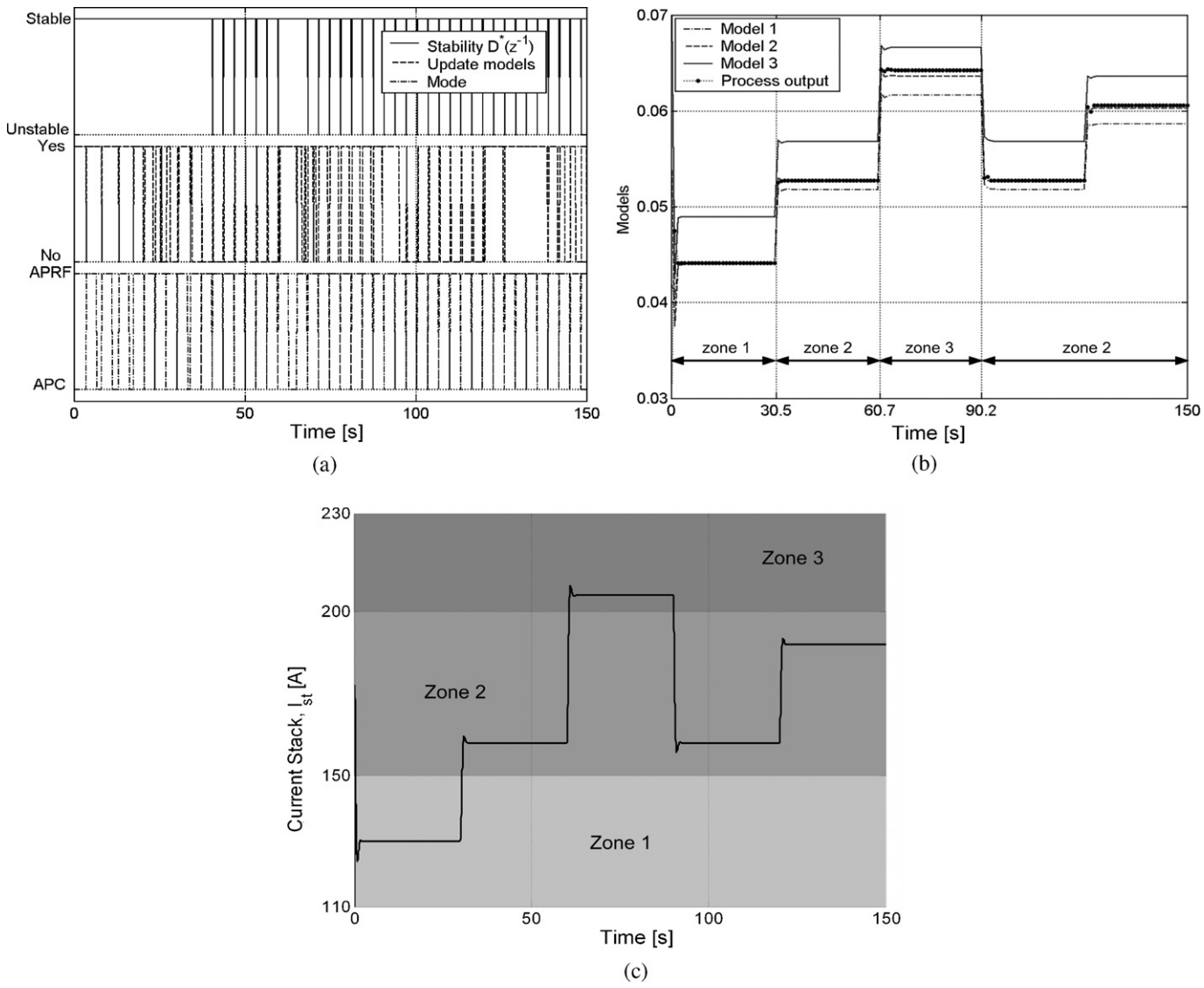

Fig. 9. Controller signals – PMDC motor. (a) Synchronization signals, (b) model predictions (compressor air flow), and (c) stack current.

analytically calculated as a linear optimization problem without restrictions.

Eq. (15) can be expressed as

$$J(k) = \mathbf{e}^T(k)\mathbf{A}^2\mathbf{e}(k) + \hat{\mathbf{u}}^T(k)\mathbf{B}^2\hat{\mathbf{u}}(k) \tag{16}$$

Then the control law can be obtained by means of $\partial J/\partial u = 0$ and considering that only the first component of the optimal future control actions vector will be applied $\hat{\mathbf{u}}(k)$ in this sampling time.

As it can be observed from Eq. (16) this structure is suitable for the design of adaptive predictive controllers (APC) by making an on line adaptation of the linear FIR model. Using, for example, recursive least-squares identification with forgetting factor and UD-factorization a suitable APC algorithm can be developed (Jordán, 1991; Jordán et al., 2006; Zumoffen et al., 2007). The overall control scheme of this APC method is shown in Fig. 3. Here, $F(z^{-1})$ is a smoothing filter for the reference, $G(z^{-1})$ the estable real plant, $\hat{G}(z^{-1}, k)$ the plant model identified at time k, and $R(z)$ and $D^*(z^{-1})$ the controller structure resulting from solving Eq. (16).

4.2. Adaptive predictive robust filter approach

In the case of a process-model mismatch $\Delta G = G - \hat{G} \neq 0$, the parallel compensation structure provides a direct way to achieve robustness of the closed loop by including a filter in the feedback path. The basic idea consists on making a correction of the predictions given by a nominal FIR model $G_0(z^{-1})$ by means of an adaptive modification. Consider that

$$\hat{G}(z^{-1}, k) = \widehat{\Delta G}(z^{-1}, k) + G_0(z^{-1}), \tag{17}$$

where

$$\widehat{\Delta G}(z^{-1}, k) = \widehat{\Delta g}(1, k)z^{-1} + \cdots + \widehat{\Delta g}(N, k)z^{-N} \tag{18}$$

The nominal FIR model $G_0(z^{-1})$ is available by the off-line identification procedure, its coefficients are $g_0(i) = [h(i) - h(i-1)]/\Delta u(k)$ and $h(k)$ is the plant response to a step change in the control signal $u(k)$. This nominal model generates a stable controller $(D_0(z^{-1}), R_0(z), K_g)$ and rewriting the FIR model prediction as:

$$\hat{y}(k) = \sum_{i=1}^{N} \widehat{\Delta g}(i)u(k-i) + \sum_{i=1}^{N} g_0(i)u(k-i) + cgl + \eta(k) \tag{19}$$

if it is represented as a linear regression it can be found the same structure as the APC case with the same regressor $\boldsymbol{\psi}(k)$ (Jordán, 1991; Jordán et al., 2006; Zumoffen et al., 2007). The estimate

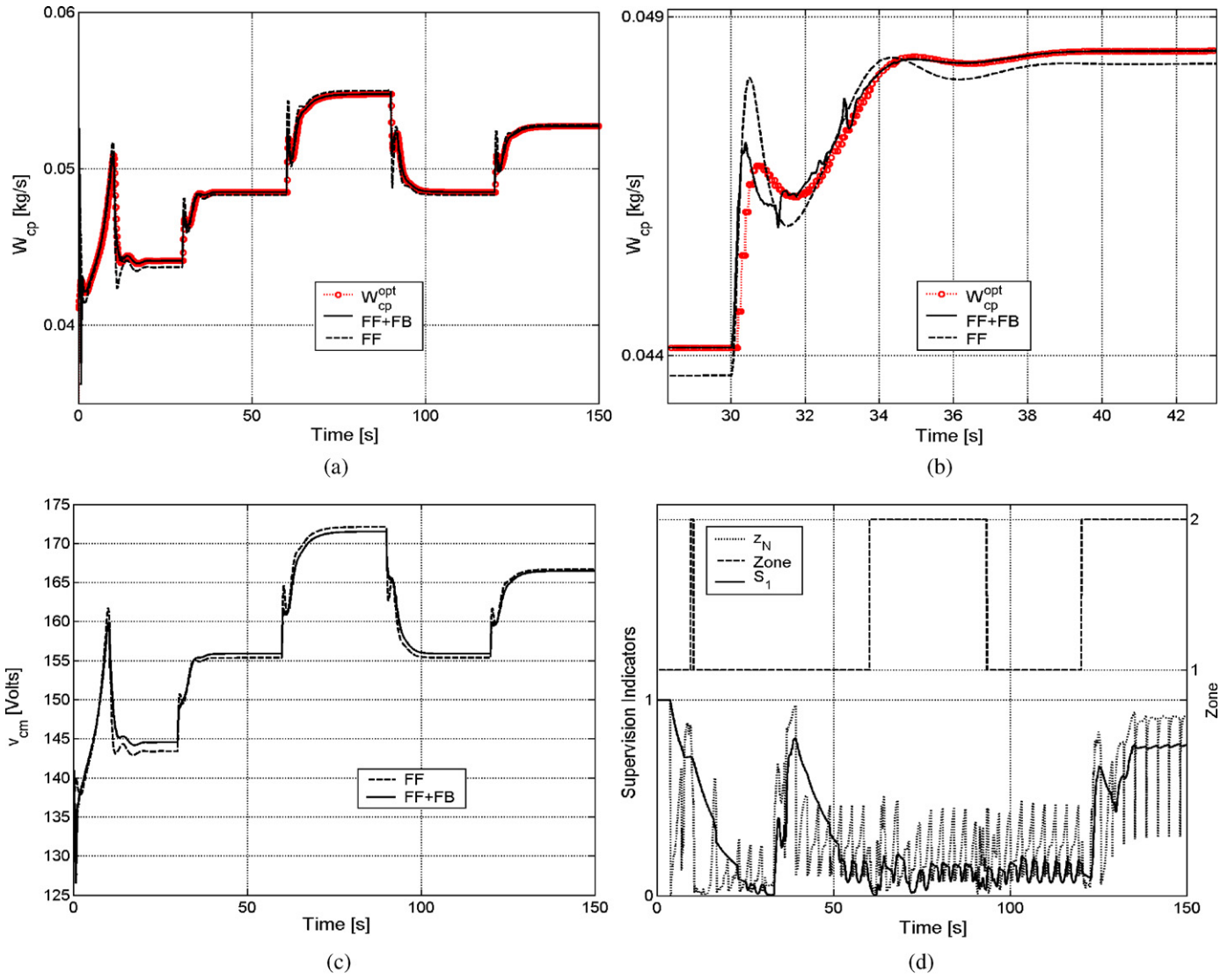

Fig. 10. Controller variables – SEDC motor. (a) Compressor air flow, (b) compressor air flow with zoom, (c) compressor motor voltage, and (d) indicators and zone.

parameter vector and the prediction error are in this case:

$$\widehat{\Delta\theta}(k) = [\widehat{\Delta g}(1,k), \ldots, \widehat{\Delta g}(N,k), \widehat{cgl}(k)]^T$$
$$\varepsilon(k) = [y(k) - y_0] - \boldsymbol{\psi}^T(k)\widehat{\Delta\theta}(k) \quad (20)$$

Then, by applying again any kind of a recursive algorithm for identification purposes, the model can be updated on-line to be used for the robust filter $\widehat{\Delta G}(z^{-1})$.

Under these conditions the static compensation must be

$$K_g(k) = \frac{1}{\widehat{\Delta G}(1,k) + G_0(1)} \quad (21)$$

This control strategy is initially based on a stable nominal controller, obtained from the nominal stable FIR model $G_0(z^{-1})$ identified off-line. By accounting Eqs. (19)–(21) and recursive identification the control structure shown in Fig. 4 can be implemented, called adaptive predictive robust filter (APRF) structure.

The asymptotic performance of the adaptive control system is, in general, better than that obtained by a robust filter system, mainly if the particular tuning coefficients allow the adaptive control to guarantee asymptotic steady state stability. Therefore, if sudden dynamic changes affect significantly the closed loop response behavior, they may be much more efficiently damped down by a robust-filter system. Additionally, an asymptotic stable and good performance behavior is achievable without extra tuning parameters. It must be noted that a suitable synchronization of both approaches is useful in order to share the advantages of both modes (Jordán et al., 2006).

4.3. Adaptive predictive control with robust filter

In order to improve the performance a proper synchronization between both, the adaptive predictive control and the adaptive robust filter approaches, has to be done. It is carried out by means of an appropriate indicator function (*mode*) that enables the commutation between both algorithms automatically. In Fig. 5 a block diagram of this approach, named adaptive predictive control with robustness filter (APCWRF) is shown.

It is well known that adaptive control systems may suffer from long-term instability when the manipulated variable $u(k)$ is not rich enough in order to ensure a good persistent excited regressor $\boldsymbol{\psi}(k)$ in the space $\Re^N$. In order to supervise if this condition is done, the use of proper indicators is recommended in case it would be necessary to stop the estimation at any time. For instance, the eigenvalues evolution of $P(k) = U_*(k)D_*(k)U_*^T(k)$ or $D_*(k)$ is found suitable to detect a future degradation of the estimates $\hat{\theta}(k)$; where $P(k)$ is the

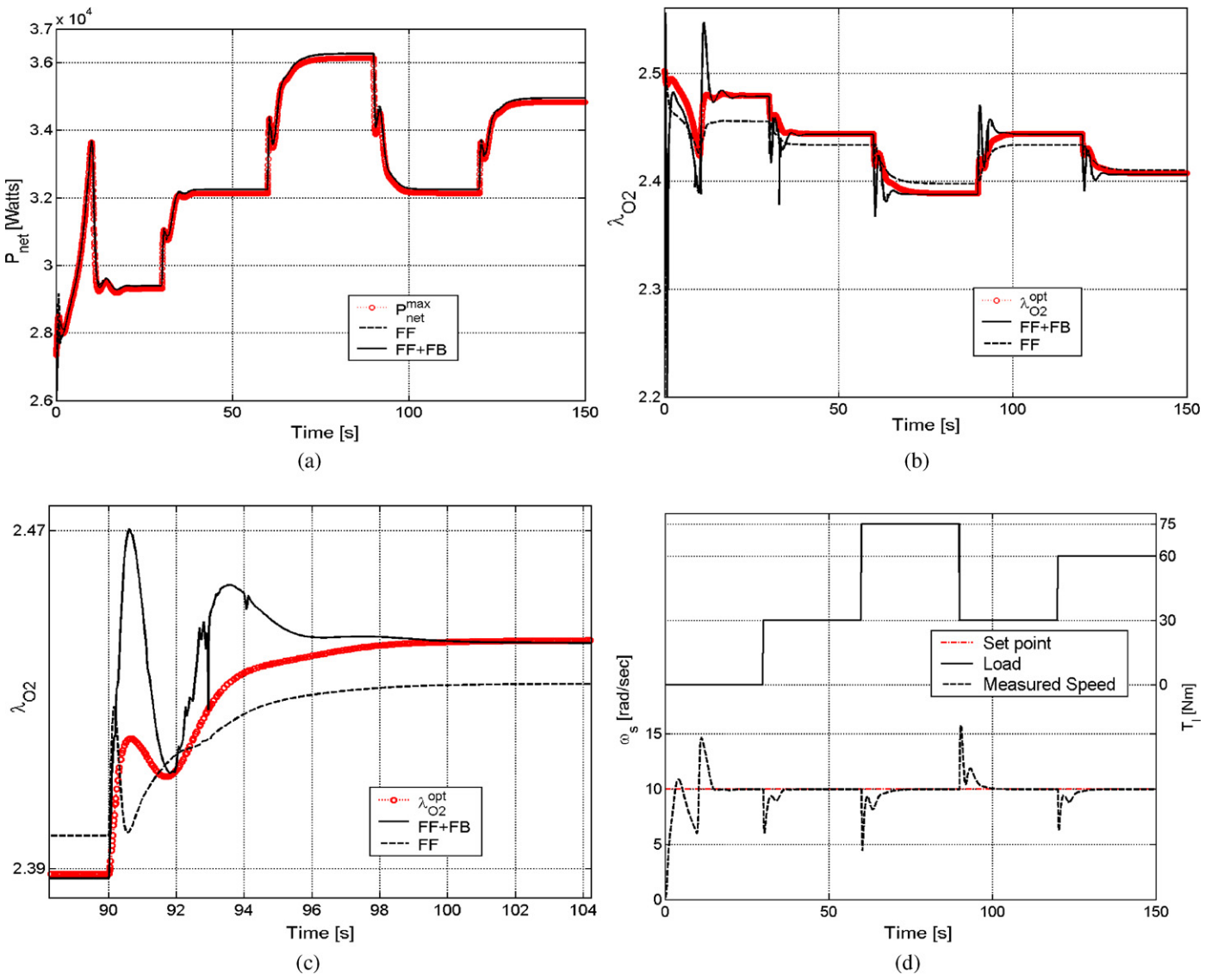

Fig. 11. Performance and load variables – SEDC motor. (a) Net power, (b) excess ratio, (c) excess ratio with zoom, and (d) shaft speed and torque.

predicition error covariance matrix. Another useful indicator is the real variable (Kofahl, 1992; Jordán et al., 2006)

$$z_N = \frac{\lambda}{\lambda + \boldsymbol{\psi}^T(k)U_*(k-1)D_*(k-1)U_*^T(k-1)\boldsymbol{\psi}(k)} \tag{22}$$

where $0 \leq z_N \leq 1$, indicating a good excited system when it is close to 0, and poorly excited when it is next to 1. In addition the second indicator defined as it is shown in Eq. (23) is very useful (Kofahl, 1992; Jordán et al., 2006)

$$s_1(k) = \begin{cases} 0.7s_1(k-1) + 0.3z_N^2(k), & \text{if } s_1(k-1) \leq 0.8z_N(k) \\ 0.99s_1(k-1) + 0.01z_N^2(k), & \text{otherwise.} \end{cases} \tag{23}$$

Finally a set of equations are available for screening if the excitation quality was enough for deciding to update or not the vector of parameters. In addition a supervision of the control loop stability in adaptive predictive control mode must be done. It can be made by analyzing the roots of the polynomial $D^*(z^{-1}, k)$ at each sampling time. Thus, a complete set of conditions for developing the synchronization rule is given.

In Fig. 6 a representative flow chart of how the synchronization algorithm works is shown. The binary variable *mode* indicates which control algorithm must be executed. For each step time, the *mode* variable is analyzed, $mode = 0$ indicates that the APC approach has been executed in the previous step time, before following in this approach the stability of the controller $D^*(z^{-1}, k)$ is evaluated. If it is stable then, the excitation degree is checked through the condition $z_N(k) < s_1(k)$ and if it is true the APC approach is run again in the next sampling time and the controller matrices are updated. On the other hand, if the polynomial $D^*(z^{-1}, k)$ is unstable or the excitation degree is not enough, the APC algorithm is switched off and the APRF approach begins working with the $mode = 1$ indicating this situation. The APRF algorithm runs during a specific period (N samples) before returning to the APC approach and update the controller matrices. The recursive estimation of the complete FIR model is avoided in case of poor excitation degree, under this condition APRF is switched on. In the APRF method a nominal stable controller is used together with the nominal FIR model (both computed off-line). In this case the recursive estimation of the model residuals is always made without considering the excitation degree, since slight modifications around the nominal FIR model are performed. In Fig. 5 can be seen the block diagram corresponding to the adaptive predictive control with robust filter (APCWRF). The interconnection of the two methods is carried

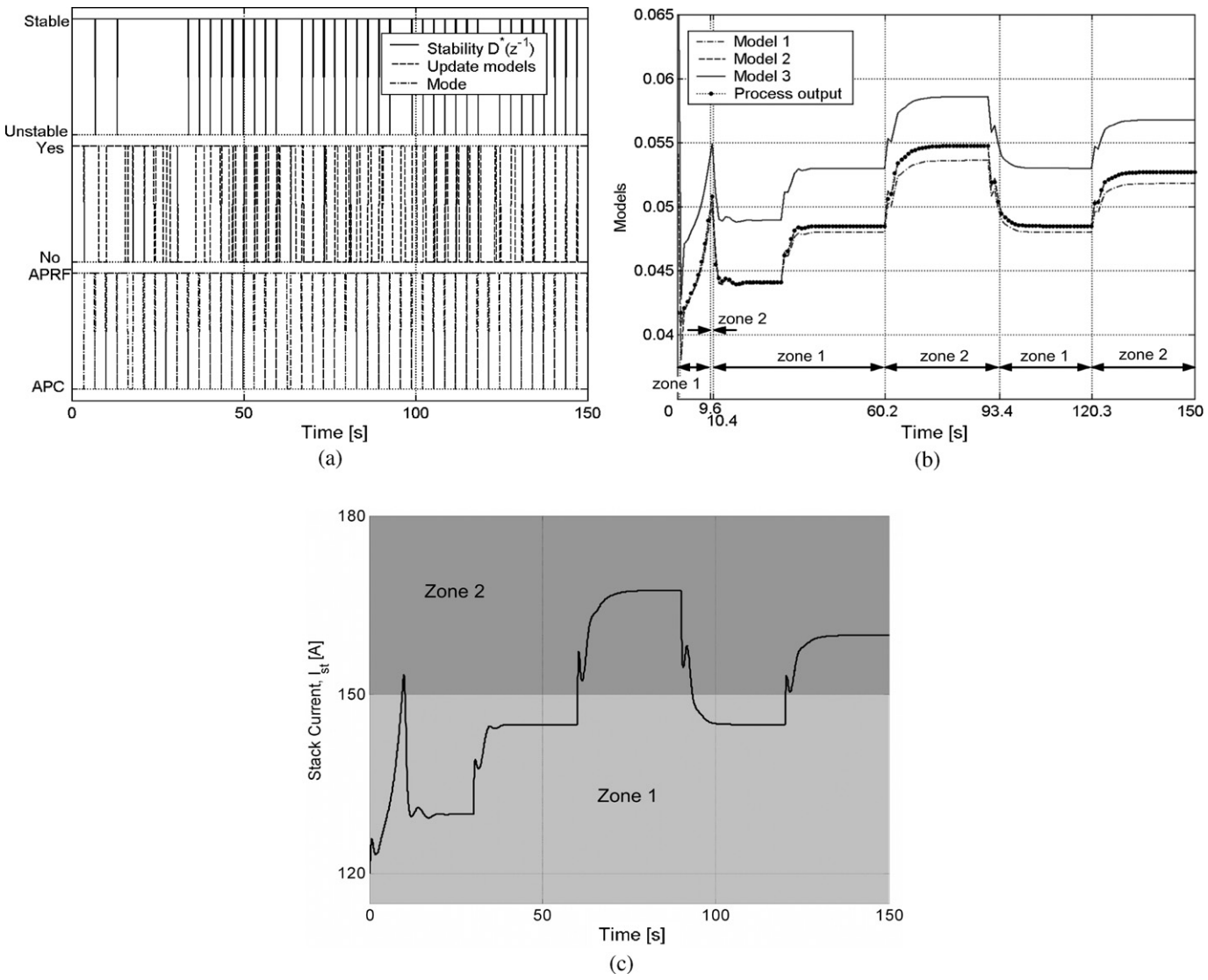

Fig. 12. Controller signals – SEDC motor. (a) Synchronization signals, (b) model predictions (compressor air flow), and (c) stack current.

out by the synchronization structure shown in Fig. 6. The final control strategy applied to the PEM is displayed in Fig. 5. The block identified as *Controller Reconfiguration* receives the information about the different operating range which is indicated by *zone*.

The commutation to APRF approach gives better robustness characteristics specially when sudden changes occur (faults, important operating point modifications, large disturbance magnitudes, etc.). Meanwhile, APC approach is mainly suitable under small dynamic changes and normal operation conditions. When the APCWRF algorithm commutes from APRF to APC approach the controller matrices are updated (R and D^*) and the stability is checked. The need for running the APRF during N iterations (the same as the FIR model order) is performed so as the regressor vector be entirely updated. Therefore, it is guarantied that the complete FIR model is updated.

The process range operation is divided in three zones, therefore three FIR nominal models are defined for each one. The commutation between the zones is handled by the current stack (I_{st} disturbance) excursions. The set point (reference trajectory) for W_{cp} is a static function of I_{st} according to Eq. (11). Thus, the commutation between zones involves selecting the corresponding model and controller parametrization, which is performed together with a set point modification in the same direction. This methodology allows a smooth dynamic behavior when sudden changes in the tracking and prediction error occur and prevents abrupt transitions in the manipulated variable. Hence, only slight transient effects during the commutation stage can be detected.

The stability aspects about the classical APCWRF approach has been discussed in Jordán (1991) and Jordán et al. (2006). In this work, the stability performance of APCWRF by zones is guarantied by a suitable initialization of the algorithm when a commutation must be performed. Each zone is characterized by a nominal stable FIR model together with a stable control structure (Fig. 5) parametrization. Thus, when a zone change takes place the actual control problem commutes to another one previously defined by their corresponding nominal FIR model and stable controller. In other words, the overall problem can be seen as three asymptotic stable APCWRF control problems. Anyway, the switching control strategies are still an open and challenging problem for medium and large scale processes.

5. Application results

In this section several simulation results are included in order to demonstrate the potentiality of the control strategy described above. Firstly, a brief comment about the controller tuning param-

eters is performed. For the case study given here, both control strategies (APC and APRF) have the same parameters shown in Table 1. The prediction horizon $[H_p, H_w]$ was adopted as 10 samples with $H_w = 1$ and $H_p = 11$ because it provides a good trade-off between transient response and prediction quality. These parameters have direct implications in the performance since when H_w presents small values produces transient effects in the predictions. Otherwise, for large values, the effect is mainly observed in the steady-state behavior. Furthermore, if the process presents dead time and/or inverse response, the prediction horizon must begin after the delay and/or the period with inverse response so as to spend less control energy. The end of the prediction horizon, H_p, has direct impact on the stability. Large values of H_p allow to have an extended vision of the future behavior so corrective actions can be taken immediately. The main problem involved with these parameters selection is the computational cost associated with them. The control horizon, H_u, in this case was selected as 2 movements. In this case allowing fewer number of movements (small control horizon) means more quick and aggressive response. Another important parameter is the FIR model order, N, in this case was adjusted to 30 samples. A practical rule of thumb (Jordán, 1991) suggests no more than 40 samples, once the sampling time, T_s, is adopted. The predictive functional cost is also parameterized by the penalty coefficients α_i and β_i which weigh the prediction error and the control energy respectively. In the matrix form these penalty coefficients are $\mathbf{A} = \text{diag}(\alpha_{H_w}, \ldots, \alpha_{H_p})$ and $\mathbf{B} = \text{diag}(\beta_0, \ldots, \beta_{H_u-1})$. In this case these matrices are adjusted to an unitary diagonal matrix and a cero matrix respectively weighing only the prediction error. The tuning implications of these matrices are direct and opposite, large values of $\mathbf{A}$ generate aggressive responses and large values of $\mathbf{B}$ produce smooth manipulated movements. Finally, the parameter referred to the recursive estimation is the forgetting factor, λ. This produces an exponential weighting of the data in the recursive algorithm. A rule of thumb (Ljung, 1999) suggests that typical values are in the range [0.96, 0.995], clearly this selection affects the convergence rate of the adaptive identification.

The results are grouped in two sets. Initially, the PMDC motor under the load disturbance profile of Eq. (14) is presented in Figs. 7 and 8. Figs. 10 and 11 summarize the same simulation condition but, in this case, connected to the SEDC motor. In both cases, the TCS guarantees the desired shaft speed of 10 rad/s under several load changes. In addition, graphical and numerical comparisons between the control strategy proposed here and the optimal static feedforward responses are included.

Fig. 7 summarizes the principal variables involved in the fuel cell control strategy. Firstly, in Fig. 7(a) can be observed the optimal compressor air flow, W_{cp}^{opt}, set point, derived from the instantaneous, I_{st} (Eq. (11)) and the measured air flow, W_{cp}, when both a static feedforward (FF) and a FF in combination with the APCWRF approach (FF + FB) are implemented. Clearly, the static FF presents offset problems and considerable overshoot in some responses. The FF + FB strategy proposed here displays a suitable behavior without offset and reduces the aggressive evolutions on, W_{cp}. It can be observed too in Fig. 7(c) where the manipulated variable, ν_{cm}, profile is presented for both control structures. Fig. 7(d) shows the principal variables in the APCWRF approach, the supervision indicators of Eqs. (22) and (23), for deciding the use of the robust filter or not, and the operating zone evolution that drives to the proper FIR model selection.

Furthermore, in Fig. 8 can be seen both, the fuel cell performance and TCS variables with the PMDC motor too. The fuel cell net power, P_{net}, in Fig. 8(a) shows a good behavior in agreement with the optimal reference (Eq. 13). Although, the net power is an indirect controlled variable (ICV), in this case both FF and FF+FB control strategies present a suitable performance. Another ICV is the excess ratio of the amount of oxygen, λ_{O_2}. The desired evolution of this variable is represented by the optimal one corresponding to that given in Eq. (12). Fig. 8(b) shows these behaviors when both, the FF and FF + FB control strategies, are implemented. Clearly, the FF approach presents important offset problems degrading its performance. Meanwhile, the FF + FB strategy allows a suitable excess ratio evolution (without offset problems) guaranteeing the optimal one even though the pass through different operating conditions. Fig. 8(d) displays the principal variables in the TCS, the load torque changes and the controlled shaft speed under this condition.

On the other hand, Fig. 9 summarizes different useful signals tied to the controller. Fig. 9(a) shows the synchronization signals used in the APCWRF approach (shown in Fig. 6) during the simulated experiment, it can be seen the stability check of $D^*(k^{-1})$, the FIR model update permission and the switching mode variable related to the used control approach along the time. Fig. 9(b) displays the three nominal FIR models prediction of the compressor air flow along the different working zones. Each model is the most representative on the corresponding zone. The stack current, I_{st}, excursions are shown in Fig. 9(c). This variable defines when the zone changes happen for the controller. It is important to note that in the limit of two zones the nominal FIR model corresponding to each one could be proper because of the given good predictions by both of them. In any case, the zones definition were made thinking on covering a wide range of the stack current excursions. This may be the case when, for example, more demanding torque loads are applied to the motors.

The second group of simulations considers the same operation conditions but in this case using a SEDC motor in the TCS. Fig. 10 presents the principal variables involved in the fuel cell control strategy. Firstly, in Fig. 10(a) can be observed the optimal compressor air flow, W_{cp}^{opt} and the measured air flow, W_{cp}, when both FF and FF + FB control are implemented. The static FF presents offset problems respect to the optimal reference trajectory. The FF + FB strategy proposed here demonstrates a suitable behavior without offset, handling well the plant-model mismatch and nonlinear problem by adaptation. This can also be observed in Fig. 10(c) where the manipulated variable, ν_{cm}, profile is presented for both control structures. Fig. 10(d) shows the principal variables in the APCWRF approach, the supervision indicators of Eqs. (22) and (23) and the pass through the different operating zones that determines the corresponding FIR model selection (and switch).

The last simulation presented in Fig. 11 displays both the fuel cell performance and TCS variables with SEDC motor. The fuel cell net power shown in Fig. 11(a) presents a good evolution in agreement with the given optimal reference (Eq. (13)) with both control structures. The net power and the excess ratio of the amount of oxygen are ICVs and are strongly related to the way that the compressor air flow is able to follow the optimal profile. In fact, the FF strategy presents considerable offset to control W_{cp} as can be observed in Fig. 11(b). Meanwhile, the suitable control of W_{cp}, made by the FF + FB approach, guarantees a correct evolution keeping the λ_{O_2} very close to the optimal trajectory. Fig. 11(d) displays the main variables in the TCS, the load torque changes and the controlled shaft speed under this condition.

Finally, Fig. 12 summarizes different useful signals tied to the controller. Fig. 12(a) shows the synchronization signals used in the APCWRF approach (Fig. 6) along the simulation, such as the stability check of $D^*(k^{-1})$, the FIR model update permission and the mode variable (defining the used control approach). Fig. 12(b) displays the three nominal model predictions of the compressor air flow along the different working zones. The stack current, I_{st}, excursions define when the zone changes happen to be processed by the controller, they are shown in Fig. 12(c).In this case the working points pass through the zones 1 and 2.

Table 2
Performance index – IAE.

Variable	PMDC motor		SEDC motor	
	FF	FF + FB	FF	FF + FB
Wcp (kg/s)	0.113	0.033	0.052	0.017
P_{net} (W)	2.72×10^4	2.55×10^4	1.80×10^4	1.17×10^4
λ_{O_2}	3.408	1.335	1.70	1.005

The most important variables such as the compressor air flow, the net power and the excess ratio are evaluated using the integral absolute error (IAE) between their instantaneous evolutions and their corresponding optimal references. The results are shown in Table 2 for both control structures, FF and FF + FB and both kind of motors. Clearly, the approach proposed here presents an improvement in this performance index assuring the correct operation of the PEMFC.

6. Conclusions

From the simulated results it is clear that the improved APCWRF is able to handle well the PEM requirements in a wide range of working zones produced by exigent load demands of different electric motors. The APCWRF presents a good performance and achieves the proposed objectives set for the complete system (PEMFC connected to the electric motors). The combined action with the feedforward contribution allows the APCWRF be able of presenting a well regulator behavior even though the complex disturbance scenarios. In addition, the feedforward action is useful for setting the optimal compressor input voltage as a function of the demanded load. Other important advantage is that indirect controlled variables (ICVs) named as "performance variables" can be kept close to the optimal values according to the imposed load changes. This preliminary result stimulates a future work where it will be considered the complete prototype including the fuel processor system which transforms bio-ethanol into hydrogen for feeding the PEMFC connected with different kind of electric motors.

Acknowledgements

The authors want to acknowledge the financial support from CONICET (Consejo Nacional de Investigaciones Científicas y Técnicas) and ANPCYT (Agencia Nacional de Promoción Científica y Técnica) from Argentina.

References

Benziger, J., Chia, E., Moxley, J., & Kevrekidis, I. (2005). The dynamic response of PEM fuel cells to changes in load. *Chemical Engineering Science*, *60*, 1743–1759.

Biset, S., Nieto Deglioumini, L., Basualdo, M., Garcia, V. M., & Serra, M. (2009). Analysis of the control structures for an integrated ethanol processor for proton exchange membrane fuel cell systems. *Journal of Power Sources*, *192*(1), 107–113.

Caux, S., Lachaize, L., Fadel, M., Shott, P., & Nicod, L. (2005). Modelling and control of a fuel cell system and storage elements in transport applications. *Journal of Process Control*, *15*, 481–491.

Gruber, J., Doll, M., & Bordons, C. (2009). Design and experimental validation of a constrained MPC for the air feed of a fuel cell. *Control Engineering Practice*, *17*(8), 874–885.

Grujicic, M., Chittajallu, K., Law, E., & Pukrushpan, J. (2004). Model-based control strategies in the dynamic interaction of air supply and fuel cell. *Proceedings of the Institution of Mechanical Engineers, Part A: Journal of Power and Energy*, *218*, 1–13.

Grujicic, M., Chittajallu, K., & Pukrushpan, J. (2004). Control of the transient behaviour of polymer electrolyte membrane fuel cell systems. *Proceedings of the Institution of Mechanical Engineers, Part D: Automobile Engineering*, *218*, 1–12.

Jayasankar, B., Ben-Zvi, A., & Huang, B. (2009). Identifiability and estimability study for a dynamic solid oxide fuel cell model. *Computers and Chemical Engineering*, *33*, 484–492.

Jordán, M. (1991). *Digitale Adaptive Regelung mit linearen nichtparametrischen Modellen*. PhD thesis. Technische Hochschule Darmstadt, Germany, VDI-Fortschrittsberichte, Reihe 8, Bd. 240, VDI Verlag GmbH, Düsseldorf.

Jordán, M., Basualdo, M., & Zumoffen, D. (2006). An approach to improve the performance of adaptive predictive control systems: Theory, simulations and experiments. *International Journal of Control*, *79*, 1216–1236.

Kofahl, R., Isermann, R., Lachmann, K. H., & Matko, D. (1992). *Robustness in parameter adaptive control. Chapter XIII. Adaptive control systems*. New York: Prentice Hall.

Ljung, L. (1999). *System identification, theory for the user*. New Jersey: Prentice Hall.

Nieto Deglioumini, L., Biset, S., Domínguez, J. M., & Basualdo, M. (2009). Control Oriented Dynamic Rigorous Model of a Fuel Processor System and Fuel Cell Stack. In *Proceedings of 10th International Symposium on Process Systems Engineering (PSE)* (pp. 609– 614). Brazil.

Pukrushpan, J., Stefanopoulou, A., & Peng, H. (2004). *Control of fuel cell power systems: principles, modeling, analysis and feedback design*. Springer.

Woo, C., & Benziger, J. (2007). PEM fuel cell current regulation by fuel feed control. *Chemical Engineering Science*, *62*, 957–968.

Wua, W., Xu, J., & Hwang, J. (2009). Multi-loop nonlinear predictive control scheme for a simplistic hybrid energy system. *International Journal of Hydrogen Energy*, *34*(9), 3953–3964.

Yang, Y., Liu, Z., & Wang, F. (2008). An application of indirect model reference adaptive control to a low-power proton exchange membrane fuel cell. *Journal of Power Sources*, *179*, 618–630.

Zenith, F., & Skogestad, S. (2007). Control of fuel cell power output. *Journal of Process Control*, *17*, 333–347.

Zhang, J., Liu, G., Yu, W., & Ouyanga, M. (2008). Adaptive control of the airflow of a PEM fuel cell system. *Journal of Power Sources*, *179*, 649–659.

Zumoffen, D., Basualdo, M., Jordán, M., & Ceccatto, A. (2007). Robust adaptive predictive fault-tolerant control integrated to a fault detection system applied to a nonlinear chemical process. *Industrial & Engineering Chemistry Research*, *46*, 7152–7163.